Influence of Si content on the structure and internal stress of the nanocomposite TiSiN coatings deposited by large area filtered arc deposition

2009 J. Phys. D: Appl. Phys. 42 125415

(http://iopscience.iop.org/0022-3727/42/12/125415)

J. Phys. D: Appl. Phys. **42** (2009) 125415 (7pp) doi:10.1088/0022-3727/42/12/125415

Influence of Si content on the structure and internal stress of the nanocomposite TiSiN coatings deposited by large area filtered arc deposition

Y H Cheng[1,5], T Browne[1], B Heckerman[1], P Gannon[2], J C Jiang[3], E I Meletis[3], C Bowman[4] and V Gorokhovsky[4]

[1] American Eagle Instruments, Inc., 6575 Butler Creek Rd, Missoula, MT 59808, USA
[2] Chemical and Biological Engineering, Montana State University, Bozeman, MT 59717, USA
[3] Materials Science and Engineering Program, University of Texas at Arlington, Arlington, TX 76019, USA
[4] Arcomac Surface Engineering, LLC, 151 Evergreen Dr., Suite D, Bozeman, MT 59715, USA

E-mail: ycheng@am-eagle.com and yh_cheng@yahoo.com

Received 21 January 2009, in final form 5 May 2009
Published 5 June 2009
Online at stacks.iop.org/JPhysD/42/125415

Abstract
TiSiN coatings were deposited by using a large area filtered arc deposition technique from TiSi targets with different Si content. The influence of the Si content in the targets on the surface morphology, composition, bonding structure, crystalline structure and internal stress of the TiSiN coatings were systematically studied by using scanning electron microscopy, x-ray photoelectron spectroscopy, x-ray diffraction and the substrate curvature method, respectively. It was found that by increasing Si content in the TiSi targets to 20 at%, the Si content in the coatings increases linearly to 7.7 at%. Both XRD and XPS results indicate that all the TiSiN coatings consist of a nanosized TiN phase and an amorphous Si_3N_4 phase except for the coatings with Si content of above 4.5 at%, in which 5% of amorphous $TiSi_2$ phase exists. With increasing Si content in the coating, the coatings change orientation from the (1 1 1) to the (2 2 0) preferred orientation. The TiN grain size decreases linearly to 5.4 nm with an increase in Si content up to 4.5 at%, and then increases slightly with a higher Si content in the coatings. The substrate curvature method shows that the increase in the Si content from 0 to 4.5 at% results in a rapid increase in the internal stress in the coating from 2.2 to 3.9 GPa, but a further increase in the Si content leads to a slight decrease in the internal stress in the coating. The decrease in the grain size with increasing Si content contributes to the increase in the internal stress in the TiSiN coatings.

1. Introduction

Nanocomposite TiSiN coatings, consisting of nanosized TiN grains with a size of a few nanometres embedded in an amorphous Si_3N_4 matrix, have been extensively studied in the last decade due to their unique properties, such as extremely high hardness ($\geqslant$40 GPa) due to the small grain size, excellent corrosion resistance, high thermal stability, high hardness at high temperature and excellent oxidization resistance under high temperature and oxidative environment [1–9].

Various deposition techniques, such as chemical vapour deposition (CVD) [1–3], plasma enhanced chemical vapour deposition (PECVD) [4], magnetron sputtering [5], cathodic vacuum arc [6, 7] and filtered cathodic vacuum arc [8], have been successfully used to deposit nanocomposite TiSiN coatings. Due to the high ionization rate, high ion energy, high ion current density and the capability of removing macro-particles, filtered cathodic arc is one of the most suitable

[5] Author to whom any correspondence should be addressed.

techniques for the deposition of TiSiN coatings for the industry. Recently, we successfully deposited nanocomposite TiSiN coatings from a TiSi target using the large area filtered cathodic arc deposition (LAFAD) technique, which utilizes 90° deflecting magnetic fields to deflect ions from the cathodic arc plasma to the deposition chamber and removes unwanted macro-particles generated during arc evaporation [10–13]. High current density, 5 mA cm^{-2}, and high ion energy make it possible to deposit TiSiN coatings at a low deposition temperature and a low N_2 partial pressure [8].

For TiSiN coatings, Si content in the coating is the most important parameter that determines the microstructure, bonding structure, crystalline structure and properties. Veprek *et al* [1–3] reported that TiSiN coatings deposited by the PECVD method at a temperature above 500 °C consists of nanosized TiN grains and an amorphous Si_3N_4 layer at a Si content of below 8–10 at%, but the $TiSi_2$ phase appears at a higher Si content; and at a Si content of 8–10 at%, the deposited coatings possess the smallest grain size and the highest hardness of 50–60 GPa. Nose *et al* [14] found that for the TiSiN coatings deposited by rf magnetron sputtering, the grain size and hardness reach a maximum of 35 nm and 40 GPa, respectively, at a Si content of about 5 at%, and coatings containing 8 at% Si have the highest internal stress. Meng *et al* [15] reported a continuous decrease in the hardness with increasing Si content in the TiSiN coatings deposited by magnetron sputtering. Martin and Bendavid [16] found that the coatings deposited by concurrent cathodic arc evaporation and magnetron sputtering exhibit the maximum hardness and internal stress at a Si content of about 10 at% and 6 at%, respectively. Perez-Mariano *et al* [17] found that the increase in the Si content leads to a change of orientation from the (2 0 0) preferred orientation to a random orientation for the TiSiN coatings deposited by CVD.

In this study, the LAFAD technique was used to deposit nanocomposite TiSiN coatings. TiSi alloy targets with different Si content were used to deposit TiSiN coatings with different Si content. The surface morphology, composition, microstructure, crystalline structure, bonding structure and internal stress of the deposited coatings were characterized by using scanning electron microscopy (SEM), x-ray photoelectron spectroscopy (XPS), x-ray diffraction (XRD) and the substrate bending method. The correlations between the Si content in the coating and the structure and internal stress of the TiSiN coatings were established.

2. Experiment

A LAFAD-1 surface engineering system was used to deposit TiSiN nanocomposite coatings. The detailed description of the deposition system was published in a previous paper [18]. Briefly, this system consists of one dual filtered arc source, one rectangular plasma-guide chamber, one deposition chamber, auxiliary anodes, heating system, a substrate bias system and a vacuum system. The dual filtered arc source consists of two primary cathodic arc sources utilizing round TiSi targets, which are placed opposite to each other on the side walls of the plasma-guide chamber, surrounded by rectangular deflecting coils and separated by an anodic baffle plate. The deposition temperature was controlled by heating elements. The plasma beam size for this system is about 50 cm diameter ×30 cm high. 17-4 stainless steel coupons with a resistivity of 0.08×10^{-4} Ω cm and 2 inch n-type (1 1 1) Si wafers with a resistivity and thickness of <0.005 Ω cm and 279 ± 25 μm, respectively, were used as substrates for characterizing the crystalline structure and internal stress in the coatings, respectively. 17-4 stainless steel coupons were cut from ∅12.5 mm × 30 cm bars, followed by grinding and polishing to a mirror finish surface.

The substrates were thoroughly cleaned and dried using an ultrasonic cleaning system before being loaded into the deposition chamber. Before deposition, the coupons were subjected to Ar plasma cleaning at a pressure, temperature, bias and time of 0.08 Pa, 350 °C, −250 V and 15 min, respectively, followed by the Ti ion sub-implantation at a pressure, bias and time of 0.02 Pa, 500 V and 2 min. In order to improve the adhesion of the TiSiN coatings, a TiSi–TiSiN gradient multilayer with a thickness of about 200 nm was deposited onto the coupon surface. The gradient layer was deposited by gradually increasing the N_2 content in the chamber from 0% to 100%. Following the deposition of the gradient layer, TiSiN coatings with a thickness of 2.5 μm were deposited.

A series of TiSiN coatings were deposited from TiSi alloy targets with Si content of 0, 5, 10, 15 and 20 at% to study the influence of the Si content in the coatings on the surface morphology, microstructure, crystalline structure, bonding structure and internal stress of the TiSiN coatings. The deposition parameters for TiSiN coatings are deposition pressure, 0.02 Pa; substrate bias, −40 V and deposition temperature, 350 °C.

The surface morphology of the TiSiN coatings was observed using a Hitachi S-4700 field emission SEM at the EMtrix Electron Microscopy Center, the University of Montana. The SEM was operated at 20 kV. The phase structure and the grain size of the TiSiN nanocomposite coatings were studied using a Siemens D500 x-ray diffractometer with a Cu K_α radiation source (λ = 0.154 06 nm). The accelerating voltage and the filament current were 40 kV and 30 mA, respectively.

The composition and the bonding structure of the TiSiN coatings were investigated using an XPS instrument (PHI Model 5600ci, Casa XPS Analytical Software). An Al Kα x-ray source was used for all samples. The conditions used for the survey scans were as follows: energy range, 0–1100 eV; pass energy, 160 eV; step size, 0.7 eV; sweep time, 180 s and x-ray spot size, 700 × 400 μm. For the high-resolution spectra, an energy range of 40–20 eV was used, depending on the peak being examined, with a pass energy of 10 eV and a step size of 0.05 eV.

The internal stress in the TiSiN coatings was determined by the radius of curvature technique which compares the curvatures of the bare silicon substrates and substrates coated with a film. The stress was given by Stoney's equation [19]:

$$\sigma = \frac{E_s t_s^2}{6(1-\nu_s)t_c}\left(\frac{1}{R_a} - \frac{1}{R_b}\right),$$

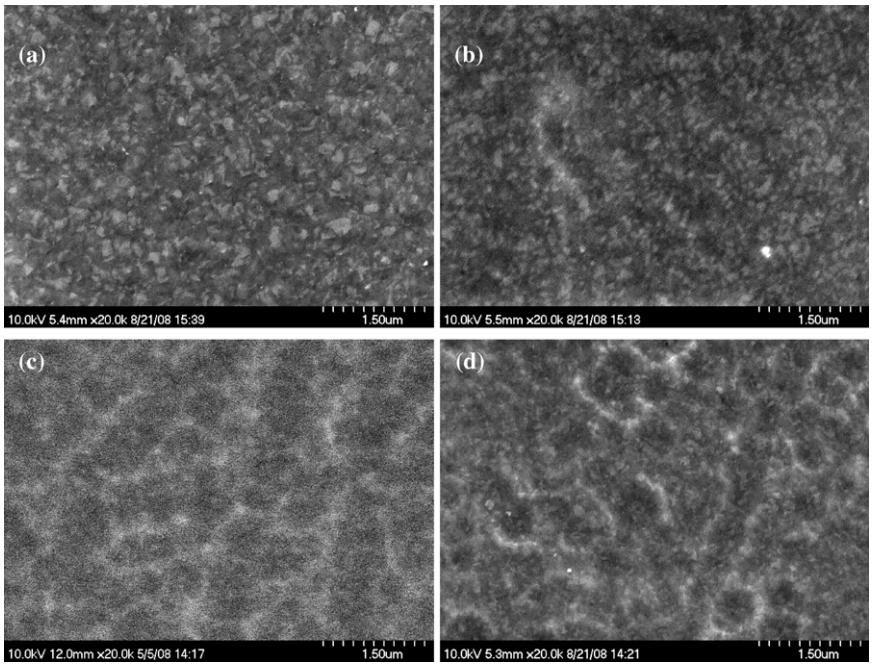

Figure 1. Typical SEM images of the TiSiN coatings deposited from TiSi targets with Si content of (*a*) 5, (*b*) 10, (*c*) 15 and (*d*) 20 at% on stainless steel substrates.

where E_s and ν_s are Young's modulus and Poisson's ratio for the substrate, t_s and t_c are the thickness of the substrate and coating, R_a and R_b are the spherical radius of curvature of the substrate after and before coating deposition, respectively. The radius of curvature of the Si wafer was measured by a contact skidless type surface profilometer (Veeco Dektak8). The stylus radius, stylus force and scan length were set to 5 μm, 10 mg and 25 mm, respectively. Before and after coating deposition, the radius of curvature of each Si wafer was measured at exactly the same location close to the wafer centre. For each wafer, three measurements were conducted. The stress shown in this paper is an average of the three measurements.

The coating thickness was measured using a Calotester (CSM). During testing, a 52100 steel ball (grade 5) with a diameter of 0.75 inch and diamond slurry with a particle size of 0.5–1 and 0–0.2 μm were used to create a wear scar. Three measurements were performed for each sample.

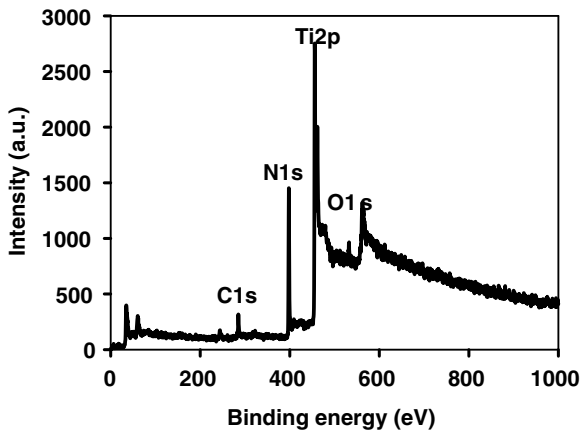

Figure 2. Typical XPS survey spectrum of the TiSiN coatings on stainless steel substrate deposited from targets with a Si content of 15 at% after Ar plasma cleaning for 5 min.

3. Results and discussion

To study the influence of Si content in the coatings on the surface morphology, TiSiN coatings deposited from the TiSi targets with different Si content were observed under SEM. Figure 1 exhibits the typical SEM images of the TiSiN coatings deposited from targets with Si content of (*a*) 5, (*b*) 10, (*c*) 15 and (*d*) 20 at% on the stainless steel substrates. It can be seen that the surface morphology of the TiSiN coatings is strongly dependent on the Si content. For the coatings deposited from the targets with 5 at% Si, the coating surface consists of faceted clusters with different shapes. The sizes of the clusters are distributed in a wide range of 100–500 nm. With the increase in the Si content in the targets to 10 at%, the clusters became much smaller and more uniform. The size of the clusters decreases to 100–200 nm, and the particles became rounded. However, the coating deposited from the targets with Si content of 15 at%, shows a completely different surface morphology, in particular a much smoother and amorphous-like morphology. For the coatings deposited from targets with 20 at% Si, the circular cluster-like structures with a size of up to 2 μm could be observed. The craters consisted of nanosized clusters with a size of 35–150 nm, which is much smaller than the cluster size on TiSiN coating deposited from the targets with Si content below 15 at%.

The composition and the bonding structure of the TiSiN coatings deposited from the TiSi targets with different Si content were investigated by XPS. Figure 2 shows a typical XPS survey spectrum of TiSiN coatings on stainless steel substrates deposited from the targets with Si content of 15 at% after Ar plasma cleaning for 5 min. As shown, after Ar plasma cleaning, the C 1s and O 1s peak intensity decreases

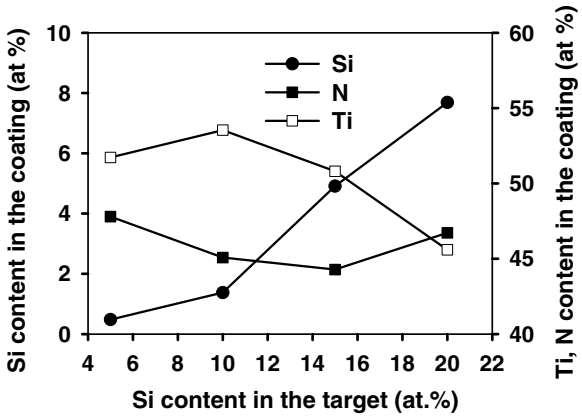

Figure 3. Dependence of the Si content in the coatings on the Si content in the TiSi targets.

dramatically to a negligible level, and two strong peaks from N 1s and Ti 2p appear [8]. This implies that the strong C 1s and O 1s peaks come from the contamination of the coating surface during the exposure of the coating to air. No Si peaks could be seen in the survey spectra, but Si 2p peaks can be detected in the fine scan spectra. Due to the low sensitivity of the instruments to Si atoms and the low concentration of Si in the coatings, the intensity of the Si peak (about 100 a.u.) is much lower as compared with the intensity of the Ti peak (about 14 049 a.u.), corresponding to the absence of the Si peak in the survey spectra. Only Ti 2p , Si 2p and N 1s peaks were included in the calculation of the coating composition.

In order to characterize the composition and the bonding structure of the TiSiN coatings deposited from the TiSi targets with different Si content, high-resolution spectra of Ti 2p, N 1s and Si 2p were collected and fitted using the Gaussian function. All spectra were calibrated using the adventitious C 1s peak with a fixed value of 284.6 eV. The background from each spectrum was subtracted and the area under each peak was used to calculate the composition of the TiSiN coatings using relative sensitivity factors from the manufacturer's handbook: Ti (1.798), N (0.477) and Si (0.283). Figure 3 shows the dependence of the Si, Ti and N content in the coating on the Si content in the TiSi targets. As shown, the Si and Ti content in the coating are strongly dependent on the Si content in the target. With the increase in the Si content in the targets from 5 to 20 at%, the Si content in the coatings increases linearly from 0.5 to 7.7 at%, but the Ti content in the coatings decreases gradually from 52 to 46 at%. With the change of Si in the targets, the N content in the coating remains almost the same in the range of 44–47 at%. As the N content in the coatings is below 50 at%, the deposited TiSiN coatings are slightly under-stoichiometric.

After comparing the Si/Ti ratio in the coatings to the Si/Ti ratio in the targets, we found that the Si/Ti ratio in the coating is much smaller, and the Si transportation efficiency, which is defined as the Si/Ti ratio in the coatings divided by the Si/Ti ratio in the targets, increases almost linearly with increasing Si content in the targets. The low Si/Ti ratio in the coatings may be attributed to the smaller charge number of Si ions. At an arc current of 100 A, the average charge numbers for Ti and Si are 2.1 and 1.4, respectively [20]. As we know, for any kind of electro-magnetic filtered cathodic arc source, the magnetic field in the filter can magnetically constrain the electrons produced by arc plasma, but are not strong enough to influence the ion trajectories to any great extent. The flow of electrons in the filter generates electrostatic fields, which guides the ions from the cathode to the substrate. As the force exerted on the ions by this electrostatic field is proportional to their charge number, the ions with a higher charge number can easily pass through the filter. As Si ions produced by arc plasma have a much lower average charge number, Si ions have a much lower ion transport efficiency through the filter, corresponding to the lower Si/Ti ratio in the coatings than that in the targets. In addition, the difference in the erosion rate of Si and Ti in the TiSi alloy targets and the emission energy of the Si and Ti ions may also contribute to the lower Si/Ti ratio in the coatings. The detailed mechanism for the change in the Si efficiency with Si content in the targets is not clear yet, but it may correlate with the change in the Si ionization rate or the charge state with increasing Si content in the targets.

Figure 4 shows the high-resolution Ti 2p (*a*), N 1s (*b*) and Si 2p (*c*) XPS spectra of the TiSiN coatings deposited from the targets with Si content of (a) 5, (b) 10, (c) 15 and (d) 20 at% on stainless steel substrates. With the increase in the Si content in the coatings, there is no significant change in the Ti 2p and N 1s line shape and position. The Ti 2p spectra consist of two main peaks at binding energies of 455.3 and 461.1 eV, as well as two shoulder peaks at binding energies of 457.1 and 463.2 eV. As a result, the Ti 2p spectra of the TiSiN coatings were fitted with four Gaussian functions as shown in this figure. As discussed in a previous paper [8], the first and second main peaks correspond to the Ti $2p_{3/2}$ splitting and their respective $2p_{1/2}$ splitting, respectively, of the TiN phase [21]. The two shoulder peaks are inherent characteristic features of the TiN phase, but it cannot rule out the contribution of the Ti–O bonds in the intermediate phases [22–24]. All the N 1s XPS spectra are characterized as a nearly symmetric peak at 397.23 eV in the binding energy range of 395–402 eV, which is slightly higher than that in the N 1s spectra of TiN (396.8 eV). The up-shift of the N 1s spectra was attributed to the synergistic effect of the oxygen, titanium and silicon atoms in the coatings [8, 22]. This indicates the existence of N–Ti, N–Si and N–O–Ti bonds. Due to the low Si and O content in the coating, most of the N atoms bonded to the Ti atoms.

The Si 2p spectra for all the TiSiN coatings exhibit a narrow peak centred at 101.47 eV in the binding range of 98–104 eV. For the coatings deposited from the targets with a Si content of 5 and 10 at%, the Si signal is very weak and exhibits a broad peak centred at 101.6 eV. With a further increase in the Si content in the coatings, the intensity of the Si 2p peaks increases continuously. After comparing curves (c) and (d), we can see that the shape of the Si 2p peak changes from symmetric to slightly asymmetric, with a shoulder peak at a low binding energy of 98.8 eV. It has been proposed that the peak at 101.47 eV originated from the Si 2p in amorphous silicon nitride (a-Si_3N_4), in which Si bonding coordination is tetrahedral (four-fold with N) [25], and the peak at 98.8 eV is assigned to $TiSi_2$ or to free Si [17]. This indicates that for the coatings with Si content of below 4.5 at%, Si atoms in the

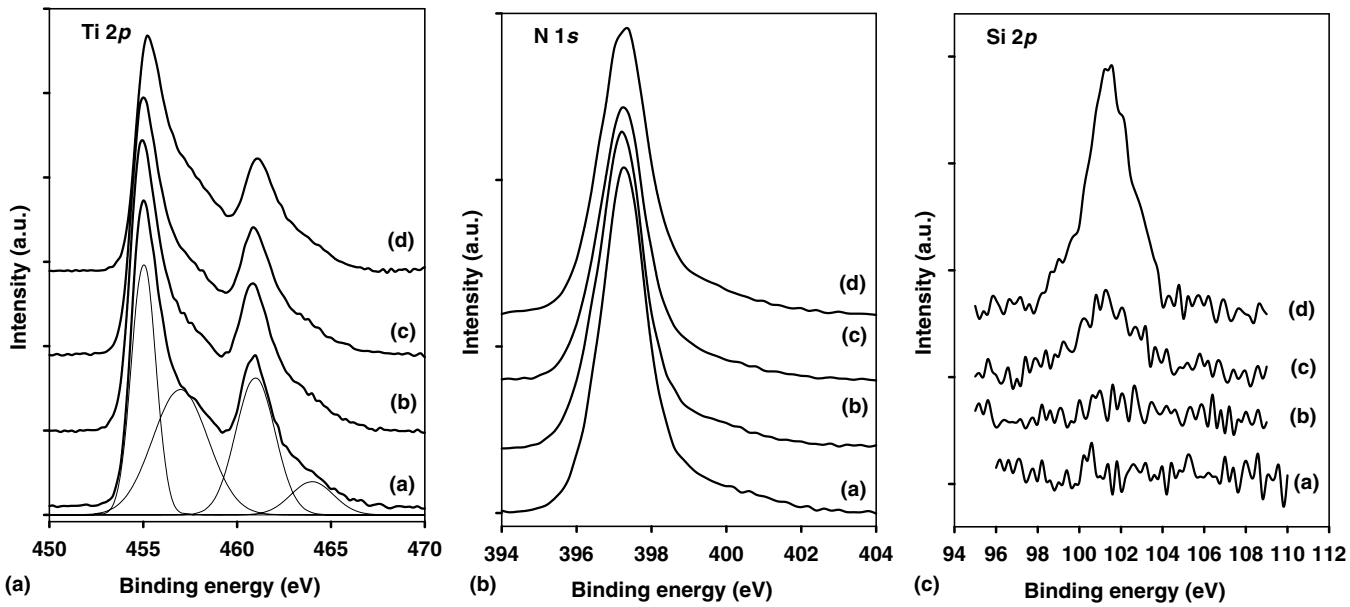

Figure 4. High-resolution Ti 2p (*a*), N 1s (*b*) and Si 2p (*c*) XPS spectra of the TiSiN coatings deposited from targets with Si content of (a) 5, (b) 10, (c) 15 and (d) 20 at% on stainless steel substrates.

coating exist as amorphous silicon nitride. However, for the coatings with a Si content of 7.7 at%, an additional $TiSi_2$ phase formed in the coatings. The deconvolution of the Si 2p peak in curve (d) shows that only 5% of Si atoms in the coatings exist as $TiSi_2$ phase.

XRD was used to ascertain the evolution of the phase structure and the grain size in the TiSiN coatings with Si content in the coatings. Figure 5 depicts the XRD patterns of the TiSiN coatings deposited from targets with Si content of (*a*) 5, (*b*) 10, (*c*) 15 and (*d*) 20 at% on the stainless steel substrates. For the coatings deposited from the targets with Si content of 5 and 10 at%, no obvious change in the XRD patterns is observed. Three peaks at 2θ angles of 36.52°, 44.80° and 77.1° are observed. According to the JCPDS 65-0965 and 06-0696 cards, it can be concluded that the first and third peaks correspond to the (1 1 1) and (2 2 2) planes of the cubic TiN phase, and the second peak corresponds to the (1 1 0) plane of the steel substrate. It is worth noting that only the (1 1 1) and (2 2 2) peaks from the TiN phase are detected by XRD, indicating that the TiN crystals in the TiSiN coatings with low Si content have a complete (1 1 1) preferred orientation. Careful inspection of figure 5(*a*) shows a very weak shoulder peak at a 2θ angle of 35.37°. This peak is assigned to the (1 0 0) plane of the hexagonal Ti phase, which comes from the Ti bonding layer. However, the XRD patterns from the coatings with high Si content, as shown in curves (*c*) and (*d*), are quite different. These show four peaks at 2θ angles of 38.00°, 44.50°, 60.64° and 64.50°. The first and third peaks correspond to the TiSi(1 0 2) plane and the TiN(2 2 0) plane, respectively. The strong TiSi(1 0 2) peaks in the curve are believed to result from the TiSi bonding layer. The second and the fourth peaks correspond to the (1 1 0) and (2 0 0) planes, respectively, of the steel substrate. As only the (2 2 0) peak from the TiN phase is observed in the XRD patterns for the coatings with high Si content, the deposited TiSiN coatings exhibit a fully (2 2 0) preferred orientation. In addition, no

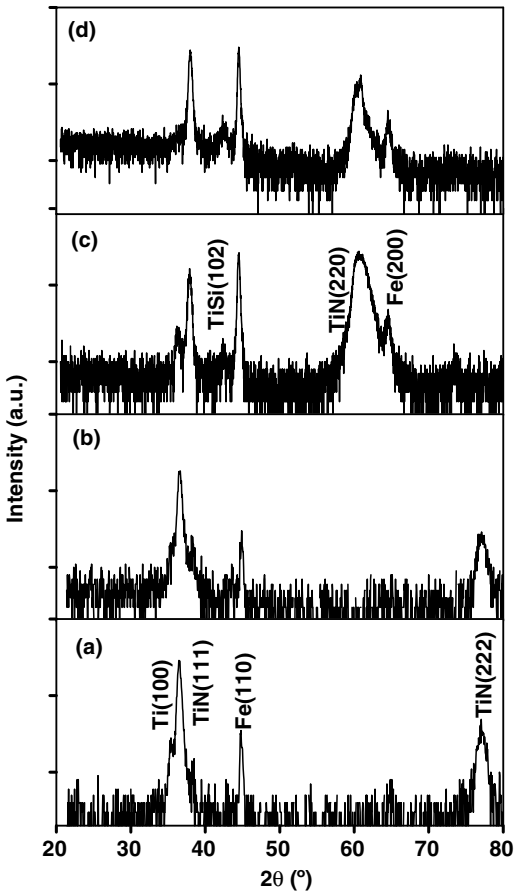

Figure 5. XRD patterns of the TiSiN coatings deposited from targets with Si content of (*a*) 5, (*b*) 10, (*c*) 15 and (*d*) 20 at% on stainless steel substrates.

diffraction peaks originate from any SiN_x phase as observed from all the XRD patterns of the TiSiN coatings. This indicates that the SiN_x phase in the coating is amorphous or nanosized crystals.

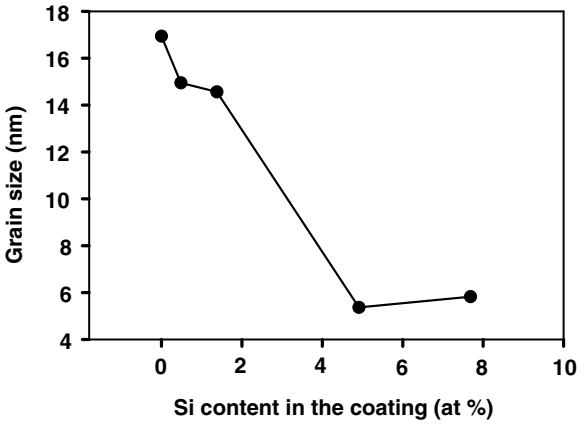

Figure 6. Dependence of the grain size on the Si content in the TiSiN coatings.

With increasing Si content in the coatings, a broadening of the XRD peaks from the TiN phase could be observed, which indicates a decrease in the grain size in the coatings. It is well known that the grain size can be computed from the full width at half maximum (FWHM) of the XRD peaks using the Scherer equation [26]: $D = \frac{0.9\lambda}{B\cos\theta}$, where D is the diameter of the grain, B is the FWHM of the diffraction peak and θ is half of the diffraction angle. As the grain size, the strain and the instrument affected the change in the observed FWHM, it is difficult to accurately calculate the grain size. FWHM of diffraction maxima was used to identify and evaluate the variation trends in the grain size with Si content in the coatings. The TiN (1 1 1) peaks in curves (*a*) and (*b*) and the TiN (2 2 0) peaks in curves (*c*) and (*d*) were fitted using the Gaussian function. The fitted FWHM was used to calculate the TiN grain size in the coatings.

Figure 6 presents the dependence of the grain size on the Si content in the TiSiN coatings. As shown, the influence of the Si content in the coatings on the TiN grain size is divided into two regimes at a Si content of 4.5 at%. The TiN grain size decreases linearly from 16.9 to 5.4 nm with increasing Si content in the TiSiN coatings from 0 to 4.5 at%. A further increase in the Si content to 7.7 at% results in a slight increase in the grain size to 5.8 nm.

Both XPS and XRD results demonstrate that the TiSiN coating deposited by the LAFAD technique consists of a crystalline TiN phase and an amorphous S_3N_4 phase. The content of the amorphous Si_3N_4 phase increases with increasing Si content in the coatings. The formation of the crystalline TiN phase and the amorphous S_3N_4 phase in the TiSiN coating results from the immiscibility of the TiN and Si_3N_4 phases, as well as the spinodal phase transformation. Although Veprek *et al* [1–3] proposed that spinodal phase segregation in the Ti–Si–N system requires sufficiently high nitrogen partial pressure (>1 Pa) and deposition temperature (>500 °C), the LAFAD technique produces high density, highly reactive and high ion energy plasma with high current density. The highly reactive nitrogen species produced by the LAFAD technique together with the atomic scale heating (ACH) generated by the bombardment of the high flux energetic ions provide the required nitrogen activity as well as the thermal energy for spinodal phase segregation [8, 27], leading to the occurrence of spinodal phase segregation at a low deposition temperature (350 °C) and low N_2 partial pressure (0.02 Pa).

During the deposition of the TiSiN coatings, due to the immiscibility of the TiN and Si_3N_4 phases, the spinodal phase transformation leads to the segregation of the amorphous Si_3N_4 phase in the grain boundary of the TiN grains. The formed amorphous Si_3N_4 phase is cohesively bonded to the TiN grains, which reduces the porosity of the grain boundaries, and therefore, hinders the diffusion of Ti atoms between the TiN grains. In addition, the low deposition temperature as well as the strong bonds formed between the Ti, Si and N atoms on the coating surface also hinders the atomic mobility. As a result, adding Si into the TiN coatings leads to a continuous decrease in the grain size as shown in figure 6. However, when the Si content in the coatings reaches percolation limits, 4.5 at%, all the TiN grains in the TiSiN coatings were encapsulated by an amorphous Si_3N_4 layer. A further increase in the Si content in the coating increases the thickness of the amorphous Si_3N_4 layer in the grain boundary and the formation of the $TiSi_2$ phase. In this case, the TiN grain size remains almost constant.

The evolution of the preferred orientation of the TiN phase in the TiSiN coatings from (1 1 1) to (2 2 0) with increasing Si content in the coatings can also be explained by the reduced mobility of Ti atoms on the coating surface and between the TiN grains. The (1 1 1) preferred orientation of the TiSiN coatings with low Si content is believed to result from the high internal stress in the coatings as the (1 1 1) plane of the TiN phase possesses the lowest strain energy [28]. The growing of the coatings with the (1 1 1) plane perpendicular to the growing direction reduces the strain energy in the coatings. As aforementioned, the addition of Si into the TiN coating reduces the mobility of Ti atoms on the coating surface by forming an amorphous Si_3N_4 layer in the grain boundary. All the TiN grains on the coatings with a Si content above 4.5 at% were covered with the amorphous Si_3N_4 layer, which confines the diffusion of Ti atoms on the coating surface. Consequently, the coatings try to grow along a less dense plane. As the TiN phase possesses a face centred cubic (FCC) structure, the (1 1 0) plane has the lowest plane density, and is the least dense plane, corresponding to the development of the (2 2 0) preferred orientation [8].

Figure 7 illustrates the internal stress in the TiSiN coatings as a function of the Si content in the coating. As shown, the increase in the Si content in the TiSiN coatings from 0 to 1.5 at% results in a drastic increase in the internal stress from 2.2 to 3.5 GPa. The internal stress in the coatings increases gradually to 3.9 GPa with a further increase in the Si content in the coatings to 4.5 at%, then decreases to 3.2 GPa with a further increase in the Si content to 7.7 at%. Veprek *et al* [1–3] and Martin and Bendavid [16] also observed a similar variation trend of the internal stress in the TiSiN coatings with increasing Si content.

In general, internal stress, including tensile and compressive stress, exists in all the coatings deposited by physical vapour deposition. Due to the high ion energy, the internal stress in the coatings deposited by filtered cathodic

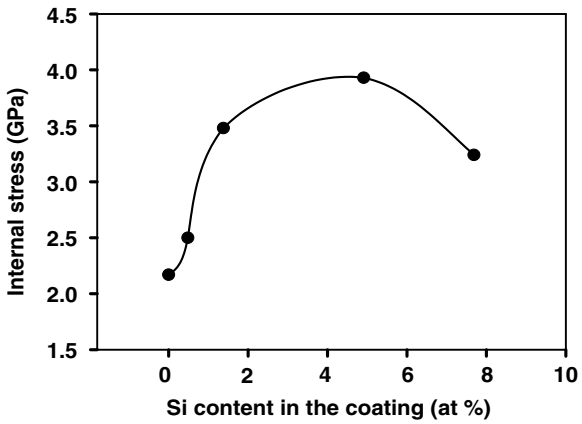

Figure 7. Internal stress in the TiSiN coatings as a function of the Si content in the coatings.

vacuum arc is usually compressive [18, 24, 28, 29]. It has been found that the internal stress in the coating is strongly dependent on the deposition parameters, including deposition temperature, substrate bias and deposition pressure. In this study, all the deposition parameters remained the same; the only variable for each coating is the Si content in the target. As discussed above, the addition of Si into the coatings led to a continuous decrease in the grain size, which increased the defect density in the coatings. It has been proposed that the internal stress in the coating is strongly correlated with the defects, which cause the deformation and distortion of the lattice [30]. The decrease in the grain size with increasing Si content in the coating corresponds to the rapid increases in the internal stress in the TiSiN coatings. The decrease in the internal stress in the coatings with higher Si content may result from the formation of a new $TiSi_2$ phase in the coating, which releases the strain in the coatings.

4. Conclusions

In this study, a novel LAFAD deposition technique was used to deposit nanocomposite TiSiN coatings from TiSi alloy targets with different Si content at a low temperature. The dependence of the composition, bonding structure, crystalline structure, grain size and internal stress on the Si content in the targets was systematically investigated. The Si content in the coating increases continuously from 0.5 to 7.7 at% with increasing Si content in the targets from 5 to 20 at%. However, the Si/Ti ratio in the coating is lower than that in the targets. XPS results show that two phases, TiN and Si_3N_4 phases, exist in the TiSiN coatings, and the content of the Si_3N_4 phases increases with Si content in the coating. In addition, a small fraction (5%) of the $TiSi_2$ phase was detected in the coatings with a Si content of 7.7 at%. XRD results indicate that only the TiN phase exists in all the TiSiN coatings; the preferred orientation changes from (1 1 1) to (2 2 0) with the increasing Si content in the coatings and the TiN grain size decreases linearly from 16.9 to 5.4 nm with increasing Si content in the TiSiN coatings from 0 to 4.5 at%, then remains with almost no change. The internal stress in the coating increases rapidly from 2.2 to 3.9 GPa with increasing Si content from 0 to 4.5 at%, then decreases slightly to 3.2 GPa with a further increase in the Si content to 7.7 at%.

Acknowledgments

The authors would like to express gratitude for the support of The United States Army Telemedicine and Advanced Technology Research Center (TATRC), US Army Medical Research & Material Command under contract number of W81XWH-08-2-0023.

References

[1] Veprek S and Veprek-Heijman M G J 2007 *Surf. Coat. Technol.* **201** 6064
[2] Veprek S, Niederhofer A, Moto K, Bolom T, Mannling H-D, Nesladek P, Dollinger G and Bergmaier A 2000 *Surf. Coat. Technol.* **133–134** 152
[3] Veprek S, Veprek-Heijman M G J, Karvankova P and Prochazka J 2005 *Thin Solid Films* **476** 1
[4] Ee Y C, Chen Z, Wang W D, Chi D Z, Xu S and Law S B 2005 *Surf. Coat. Technol.* **198** 291
[5] Li Z G, Wu Y X and Miyake S 2007 *J. Vac. Sci. Technol.* A **25** 1524
[6] Guo C T, Lee D and Chen P C 2008 *Appl. Surf. Sci.* **254** 3130
[7] Yang S M, Chang Y Y, Lin D Y, Wang D Y and Wu W 2008 *Surf. Coat. Technol.* **202** 2176
[8] Cheng Y H, Browne T and Heckerman B 2009 *J. Vac. Sci. Technol.* A **27** 82
[9] Chang C L, Lin C T, Tsai P C, Ho W Y, Liu W J and Wang D Y 2008 *Surf. Coat. Technol.* **202** 5516
[10] Gorokhovsky V I, Polistchook V P and Yartsev I M 1993 *Surf. Coat. Technol.* **61** 101
[11] Has Z, Mitura S and Gorokhovsky V 1991 *Surf. Coat. Technol.* **47** 106
[12] Gorokhovsky V I, Bhat D G and Bhattacharya R 2001 *Surf. Coat. Technol.* **140** 215
[13] Gorokhovsky V 2003 *US Patent* No 6,663,755 B2
[14] Nose M, Deguchi Y, Mae T, Honbo E, Nagae T and Nogi K 2003 *Surf. Coat. Technol.* **174–175** 261
[15] Meng W J, Zhang X D, Shi B, Tittsworth R C, Rehn L E and Baldo P M 2002 *J. Mater. Res.* **17** 2628
[16] Martin P J and Bendavid A 2003 *Surf. Coat. Technol.* **163–164** 245
[17] Perez-Mariano J, Lau K-H, Sanjurjo A, Caro J, Casellas D and Colominas C 2006 *Surf. Coat. Technol.* **201** 2217
[18] Cheng Y H, Browne T, Heckman B, Jiang J C, Meletis E I, Bowman C and Gorokhovsky V 2008 *J. Appl. Phys.* **104** 093502
[19] Stoney G 1909 *Proc. R. Soc. Lond.* A **82** 172
[20] Boxman R L, Sanders D M, Martin P J and Lafferty J M 1995 *Handbook of Vacuum Arc Science and Technology: Fundamentals and Applications* (Park Ridge, NJ: Noyes)
[21] Vesel A, Mozetic M, Kovac J and Zalar A 2006 *Appl. Surf. Sci.* **253** 2941
[22] Bertoti I 2002 *Surf. Coat. Technol.* **151–152** 194
[23] Guemmaz M, Moser A and Parlebas J C 2000 *J. Electron Spectrosc. Relat. Phenom.* **107** 91
[24] Cheng Y H and Tay B K 2003 *J. Vac. Sci. Technol.* **21** 1609
[25] Veprek S 1999*J. Vac. Sci. Technol.* A **19** 2401
[26] Klug H P and Alexander L E 1974 *X-ray Diffraction Procedures for Polycrystalline and Amorphous Materials* (New York: Wiley-Interscience)
[27] Anders A 2002 *Appl. Phys. Lett.* **80** 1100
[28] Cheng Y H and Tay B K 2003 *J. Cryst. Growth* **252** 257
[29] Cheng Y H, Tay B K and Lau S P 2002 *J. Vac. Sci. Technol.* A **20** 1270
[30] Lughi V and Clarke D R 2006 *Appl. Phys. Lett.* **24** 241911